Available online at www.sciencedirect.com
SCIENCE DIRECT®
International Journal of Heat and Mass Transfer 47 (2004) 3341–3353
International Journal of HEAT and MASS TRANSFER
www.elsevier.com/locate/ijhmt

Optimal experimental estimation of thermal dispersion coefficients in porous media

T. Metzger [a,*], S. Didierjean [b], D. Maillet [b]

[a] Fakultät für Verfahrens- und Systemtechnik, Otto-von-Guericke-Universität, Universitätsplatz 2, 39106 Magdeburg, Germany
[b] LEMTA, Institut National Polytechnique de Lorraine, 2 Avenue de la Forêt de Haye, 54504 Vandœuvre-lès-Nancy, France

Received 18 June 2003; received in revised form 23 January 2004

Abstract

In this work, thermal dispersion coefficients, as they appear in the one-temperature model, are estimated for a packed bed of glass spheres through which water is flowing with Péclet numbers up to 130. Thermocouples in the downstream neighborhood of a line heat source measure the temperature response to a step heat input. Due to experimental uncertainties in fluid velocity and thermocouple positions, ordinary least squares estimation on the thermocouple signal alone is of poor quality. Optimal experimental design and simultaneous estimation of velocities and thermocouple positions by the Gauss–Markov method—using prior (but uncertain) information on the thermocouple locations—allow for highly improved estimation of the longitudinal thermal dispersion coefficient. The lateral coefficient can only be roughly estimated by the presented method. Monte Carlo simulations of measurements allow one to assess the level of estimation errors. Excellent temperature residuals in the whole range of Péclet numbers suggest that the assumption of the one-temperature model is reasonable even in the case of local thermal non-equilibrium.

PACS: 44.30; 06.20.Dk
Keywords: Porous media; Thermal dispersion; Convective heat transfer; One-temperature model; Parameter estimation; Gauss–Markov method; Optimal experimental design

1. Introduction

Heat transport in porous media through which a fluid is flowing comprises convective and diffusive effects and is generally referred to as thermal dispersion. Its applications are numerous and range from classical ones such as fixed bed reactors in chemical engineering or underground storage of solar energy to modern ones such as the use of metal foams for the cooling of electronic circuits. A better understanding of the phenomenon is essential to improve the efficiency of these devices.

For a long time, thermal dispersion models for the average temperature were developed directly on the macroscopic scale. Based on mass dispersion models for transport in the fluid phase, they included the additional effects of fluid-to-solid heat exchange and intra-particle heat conduction. In a comprehensive review, Tsotsas [1] examined the existing types of models for longitudinal thermal dispersion: two-equation models describing the temperature evolution for fluid and solid phase separately—with either continuous or dispersed solid phase—and one-equation models for the evolution of only one average temperature for both phases. Using momentum analysis, he set up equivalence criteria between these models and derived the velocity dependence of the longitudinal thermal dispersion coefficient. Concerning lateral thermal dispersion, Bauer and Schlünder [2] have generalised a (macroscopic) mass transport model which is widely used until today.

* Corresponding author. Tel.: +49-391-6711362; fax: +49-391-6711160.
E-mail address: thomas.metzger@vst.uni-magdeburg.de (T. Metzger).

0017-9310/$ - see front matter © 2004 Elsevier Ltd. All rights reserved.
doi:10.1016/j.ijheatmasstransfer.2004.02.024

Nomenclature

a	thermal diffusivity [$m^2 s^{-1}$]
$\mathbf{a}$, $\mathbf{b}$	estimates of parameter vectors $\boldsymbol{\alpha}$, $\boldsymbol{\beta}$
c_p	heat capacity [$J K^{-1} kg^{-1}$]
d	particle diameter [m]
$\mathbf{I}_n$	identity matrix of dimension n
Pe	Péclet number ud/a_f
Q	linear heating power [$W m^{-1}$]
S	sum of squares
s	volumetric heat source [$W m^{-3}$]
$\mathbf{T}$, T	(vector of) temperature [K]
$\langle T \rangle$	average temperature [K]
t	time [s]
$\mathbf{u}_D$, u	Darcy velocity [$m s^{-1}$]
W	plane heating power [$W m^{-2}$]
$\mathbf{X}$	sensitivity matrix
$\mathbf{Y}$	measurement signal vector
$\mathbf{x}$, $\mathbf{y}$, x, y, z	(vectors of) space coordinates [m]
$:=$	equality defining a quantity

Greek symbols

$\boldsymbol{\alpha}$, $\boldsymbol{\beta}$	parameter vectors
ε	porosity
$\boldsymbol{\epsilon}$	measurement error vector
$\boldsymbol{\eta}$	theoretical model vector
λ	thermal conductivity [$W m^{-1} K^{-1}$]
λ_{eq}	equivalent thermal conductivity [$W m^{-1} K^{-1}$]
λ_x, λ_y	thermal dispersion coefficients [$W m^{-1} K^{-1}$]
$\boldsymbol{\lambda}$	thermal dispersion tensor [$W m^{-1} K^{-1}$]
$\boldsymbol{\Omega}$	weighting matrix for Gauss–Markov estimation
ρ	density [$kg m^{-3}$]
σ	standard deviation

Subscripts and superscripts

f	fluid phase
s	solid phase
T	transposed vector or matrix

More rigorous theoretical modelling starts on the microscopic scale and takes into account pore geometry and the microscopic velocity field. On the pore scale, heat transport is described by a convection–diffusion equation for the fluid phase, a diffusion equation for the solid matrix and continuity conditions for temperature and heat flux at the phase boundary. This problem cannot be solved exactly for macroscopic dimensions, and up-scaling techniques such as volume-averaging [3] or homogenization [4] need to be employed to obtain models for averaged quantities.

Carbonell and Whitaker [3] derived a two-temperature model by means of volume-averaging. Unfortunately, this most complete model contains numerous coupling parameters; these have been calculated numerically for spatially periodic porous media of simple geometry [5], but cannot be estimated experimentally for more complex structures. In order to obtain a simpler model, Carbonell and Whitaker analyzed the spatial moments of the temperature response to a one-dimensional Dirac pulse. They found that, for long times, both fluid and solid temperature signals are separated by a constant distance, which depends on geometry and thermal properties of the system as well as on fluid velocity, and that they move with the same average velocity and are dispersed at the same rate. Consequently, they obey the same convection–diffusion equation with one average velocity and one longitudinal thermal dispersion coefficient.

Recently, Moyne et al. [6] obtained a one-temperature model for thermal dispersion by using independently both volume-averaging and homogenization. They could show that this model stays valid in the case of local thermal non-equilibrium, i.e. for high fluid velocities, if the average temperature is defined as the calorimetric mean of solid and fluid average temperatures. In the same context, Da Silveira [7] carried out Monte Carlo simulations of heat transfer in two-dimensional periodic porous media with randomly created complex unit cells. By analysis of spatial moments, he obtained values for the longitudinal and lateral thermal dispersion coefficients of the one-temperature model.

Only two experimental works of major impact shall be mentioned here: Green et al. [8] estimated longitudinal thermal dispersion coefficients for a packed bed by imposing a temperature step at the inlet and measuring the response at the outlet. Levec and Carbonell [9] used the same method but largely extended the experimental range; they additionally measured lateral thermal dispersion coefficients by dividing the inlet of the packed bed into two regions, injecting hot and cold water in the respective sections and observing steady-state lateral mixing.

The aim of the present work is to estimate thermal dispersion coefficients from minimally intrusive measurements and to determine their velocity dependence. Additionally, temperature residuals are used to assess the assumption of the one-temperature model, especially for local thermal non-equilibrium. This occurs for fluid velocities corresponding to high Péclet numbers since the Péclet number represents the ratio of characteristic times for diffusion and convection on the pore scale.

2. One-temperature model for thermal dispersion

In this section, the one-temperature model as well as its solutions for two different experimental situations are presented. According to Moyne et al. [6] the average temperature $\langle T\rangle$ of the porous medium needs to be defined as the calorimetric mean of the average phase temperatures $\langle T_f\rangle^f$ and $\langle T_s\rangle^s$:

$$(\rho c_p)_t\langle T\rangle := \varepsilon(\rho c_p)_f\langle T_f\rangle^f + (1-\varepsilon)(\rho c_p)_s\langle T_s\rangle^s \tag{1}$$

where ε is the porosity of the medium and $(\rho c_p)_t$ the total volumetric heat capacity, calculated by the mixing law

$$(\rho c_p)_t := \varepsilon(\rho c_p)_f + (1-\varepsilon)(\rho c_p)_s \tag{2}$$

Then the evolution of this average temperature is described by the convection–diffusion equation

$$(\rho c_p)_t\frac{\partial\langle T\rangle}{\partial t} = \nabla\cdot(\boldsymbol{\lambda}\nabla\langle T\rangle) - (\rho c_p)_f\mathbf{u}_D\cdot\nabla\langle T\rangle + s \tag{3}$$

where $\mathbf{u}_D$ denotes the Darcy velocity, which is the volumetric fluid flow per total cross section, $\boldsymbol{\lambda}$ is the thermal dispersion tensor, which is a function of pore geometry, thermal properties and fluid velocity, and s is a volumetric heat source.

If we suppose the porous medium to be homogeneous and isotropic, and if the average fluid flow is in x-direction, i.e. $\mathbf{u}_D = (u,0,0)$, and the heat excitation s non z-dependent, then Eq. (3) simplifies to

$$(\rho c_p)_t\frac{\partial T}{\partial t} = \left(\lambda_x\frac{\partial^2 T}{\partial x^2} + \lambda_y\frac{\partial^2 T}{\partial y^2}\right) - (\rho c_p)_f u\frac{\partial T}{\partial x} + s \tag{4}$$

where T has been used to represent $\langle T\rangle$, λ_x is the longitudinal and λ_y the lateral thermal dispersion coefficient.

2.1. Transient temperature response signals

For an infinite porous medium which is initially at thermal equilibrium, i.e. at room temperature T_0 everywhere, Eq. (4) can be solved for any heat source s by successive use of an exponential transform and Green's function [10]. For a line source along the z-axis which is switched on at $t = 0$ and dissipates the constant linear heating power Q, the temperature response $\Delta T := T - T_0$ is given by

$$\Delta T(x,y,t) = \frac{Q}{4\pi\sqrt{\lambda_x\lambda_y}}\exp\left(\frac{(\rho c_p)_f ux}{2\lambda_x}\right) \times\int_0^{\frac{(\rho c_p)_f^2u^2t}{4(\rho c_p)_t\lambda_x}}\exp\left(-\left(\frac{x^2}{\lambda_x}+\frac{y^2}{\lambda_y}\right) \times\frac{(\rho c_p)_f^2u^2}{16\lambda_x}\frac{1}{\theta}-\theta\right)\frac{\mathrm{d}\theta}{\theta} \tag{5}$$

Table 1 gives the physical characteristics for a packed bed of glass spheres, as used in our experiments; two reference velocities and the corresponding values for the thermal dispersion coefficients are shown in Table 2, along with typical values for the linear heating power.

The temperature field is plotted for the small reference velocity in Fig. 1 at three different times; one can clearly see that the heated zone is dispersed in the lateral direction, but that it stays relatively confined. This confinement effect increases with velocity. Fig. 2 gives the transient temperature response for the high reference velocity at three different positions on the x-axis. Close to the heat source the temperature rise is steeper and the steady-state level higher than farther downstream, due to longitudinal and lateral dispersion respectively.

For a plane source in the y–z-plane, which dissipates the constant plane heating power W for $t > 0$, the temperature response is

$$\Delta T_{\mathrm{plane}}(x,t) = \frac{W}{\sqrt{\pi\lambda_x(\rho c_p)_t}}\exp\left(\frac{(\rho c_p)_f ux}{2\lambda_x}\right) \times\int_0^{\sqrt{t}}\exp\left(-\frac{(\rho c_p)_f^2u^2\theta^2}{4(\rho c_p)_t\lambda_x}-\frac{(\rho c_p)_t x^2}{4\lambda_x\theta^2}\right)\mathrm{d}\theta \tag{6}$$

The steady-state signal follows directly from the energy conservation law and is independent of the x-position

$$\Delta T_{\mathrm{plane},\infty} = \frac{W}{u(\rho c_p)_f} \tag{7}$$

Table 2
Reference velocities and corresponding parameter values

u (m s^{-1})	0.655×10^{-3}	6.55×10^{-3}
Pe	9.06	90.6
λ_x (W m^{-1} K^{-1})	2.4	60
λ_y (W m^{-1} K^{-1})	1	3
Q (W m^{-1})	70	300

Table 1
Physical characteristics of the porous medium (packed bed of glass spheres)

Fluid phase		Solid phase	
$(\rho c_p)_f$ (J K^{-1} m^{-3})	4.17×10^6	$(\rho c_p)_s$ (J K^{-1} m^{-3})	2.08×10^6
λ_f (W m^{-1} K^{-1})	0.607	d (m)	2×10^{-3}
a_f (m^2 s^{-1})	1.47×10^{-7}	ε	0.365

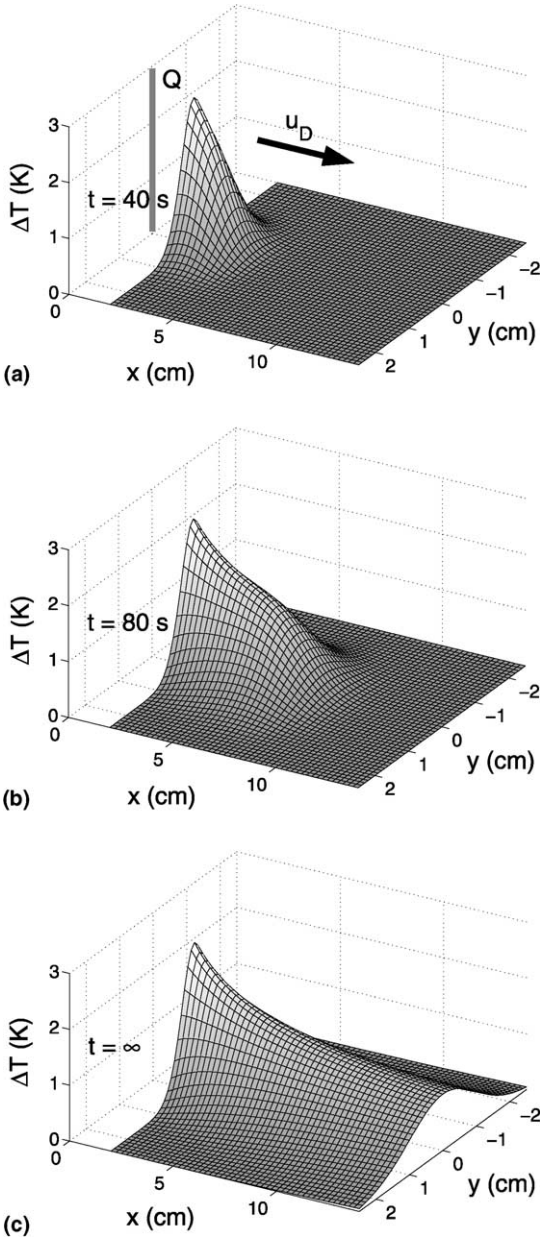

Fig. 1. Temperature field for a line heat source and $Pe = 9.06$ at different times: (a) $t = 40$ s, (b) $t = 80$ s and (c) $t \to \infty$ (for parameters see Tables 1 and 2).

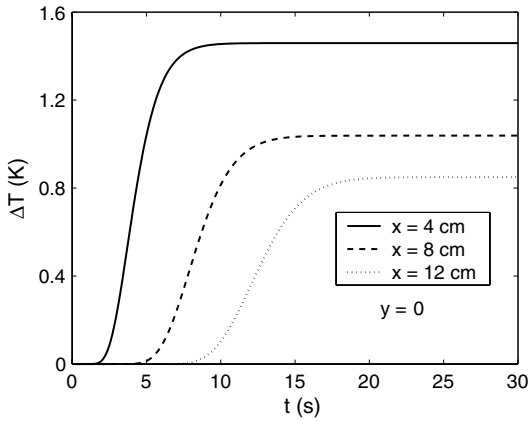

Fig. 2. Transient temperature response for a line heat source and $Pe = 90.6$ at different axial positions (for parameters see Tables 1 and 2).

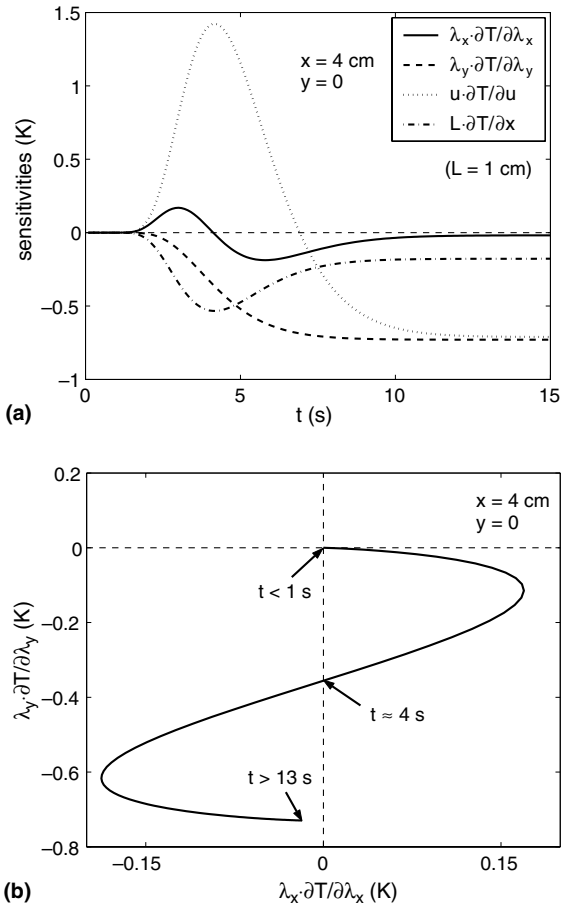

Fig. 3. Relative sensitivities for a line heat source and $Pe = 90.6$ at the axial position $x = 4$ cm (cf. Fig. 2 for the corresponding temperature signal).

2.2. Sensitivities to thermal dispersion coefficients

In order to justify the estimation of thermal dispersion coefficients from transient thermocouple measurements, relative sensitivities of the temperature signal are shown in Fig. 3a for a line heat source. It can be seen that the temperature signal is sensitive to both coefficients: the sensitivity to λ_x is low and transient (it almost

vanishes for long times) whereas the sensitivity to λ_y is higher and attains its maximum in steady state. In Fig. 3b, one sensitivity is plotted as a function of the other; this shows that they are linearly independent (otherwise the curve would be part of a line through origin) and that consequently both coefficients can be estimated at the same time.

Fig. 3a also gives the temperature signal's sensitivities to two "known" parameters, namely Darcy velocity and x-position of the thermocouple. Both sensitivities are high, meaning that small changes in these parameters have a big effect on the (measured) temperature signal. The sensitivity to the y-position of the thermocouple vanishes on the x-axis due to the symmetry of the temperature field.

3. Experimental set-up

3.1. Porous medium

The experiments are carried out in a packed bed of glass beads (with diameter $d = 2$ mm) through which water is flowing from top to bottom. In the central region of this porous medium, heating wires are installed perpendicular to water flow; Fig. 4 shows the two different installations used. Thirteen thermocouples are set in the porous medium, with their measurement junctions in the central x–y-plane and their two ends leaving in opposite z-directions.

Most thermocouples (1–7) are located on—or close to—the downstream x-axis, where the temperature signal and its sensitivities to the thermal dispersion coefficients are highest. Some (8–11) are set well off the x-axis in order to check that the heated zone stays confined and that wall effects may be neglected (cf. assumption of infinite geometry). Two thermocouples (12 and 13) are used to monitor the temperature of the incoming water T_0 and to assess the effect of natural convection for very small Péclet numbers. (Only for $Pe \leqslant 1$, thermocouple 12 measures a temperature rise. But velocity estimation, as described later, seems to show that natural convection lowers local water velocity for Péclet numbers up to 10.)

It has to be mentioned that the thermocouple wires, which are set in the empty box, are randomly displaced when the glass beads are filled in—typically by the diameter of a sphere—so that the exact measurement positions are not known. The packed bed is generated by successively filling in and compacting the beads; its overall porosity is 36.5%. The thermal properties of both phases are given in Table 1.

3.2. Linear and plane heat source

In a first series of measurements (see Fig. 4a), a single high-resistance wire (260 μm in diameter) was used as an electrical line heat source. Rough calculations for a wire in free flow showed that, within the experimental range of design parameters, boiling on the wire surface did not occur and characteristic response times were negligible. Later, mantled heating elements (of 1 mm outer diameter) were used to overcome electrical insulation problems (see Fig. 4b); however, for high Péclet numbers their response time might introduce an error in the estimation results [10].

The plane heat source is implemented by several equidistant heating elements that can produce the same temperature response in a centre region neither too close

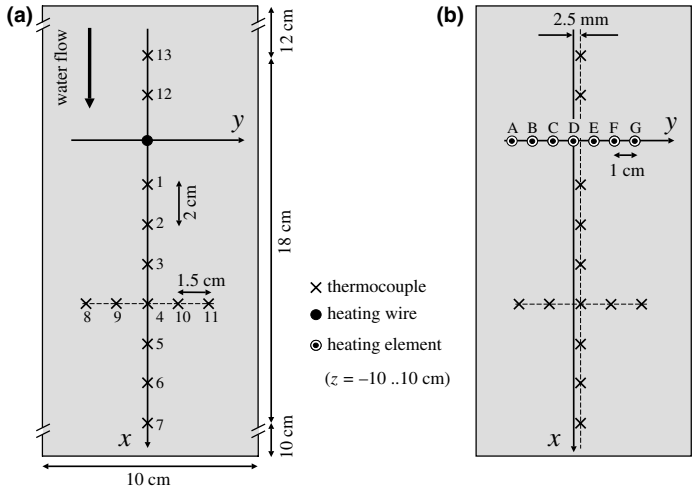

Fig. 4. Dimensions of the porous medium and positions of thermocouples relative to the heat source for (a) axial measurements and (b) off-axis measurements (with heating element D) as well as experiments with plane heat source.

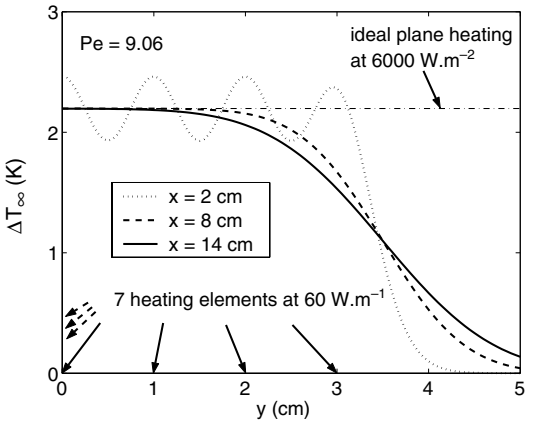

Fig. 5. Stationary temperature field ΔT_∞ for seven heating elements as in Fig. 4b at $Pe = 9.06$ and for three axial distances. (For comparison, the temperature for the corresponding plane heat source is given.)

nor too far away from the source. This is shown for the small reference velocity and steady state in Fig. 5. In the experiments, the numbers of heating elements and thermocouples were chosen according to water velocity to fulfill this criterion.

Heating power is measured electrically and monitored during all experiments; its value is chosen to have temperature signals of about 1 K and constant physical properties throughout the measurement region.

3.3. Temperature measurement

Temperature is measured by thermocouples of type E, made from wires of 127 μm diameter; their thermal response time was found to be 15 ms. The thermoelectrical voltage (between a thermally insulated reference junction and the measurement junction) is amplified 2000 times and measured at a frequency of 2 KHz; electrical noise is reduced by a first-order low pass filter of 44 Hz and by averaging data groups of 80 points (corresponding to 2 periods of 50 Hz noise). Thus, temperature can be recorded at an effective frequency of 8 Hz with a noise of about 0.01 K. Additionally, any offset of the data acquisition system or the thermocouples is corrected by the signals measured at $t < 0$.

3.4. Water flow

Water at ambient temperature is pumped from one big reservoir (200 l) through the packed bed into a separate reservoir which is floating in the first one. This is to keep the inlet temperature T_0 strictly constant and to allow the pump to operate at a constant pressure difference. The flow rate can be adjusted by valves and is monitored during the experiments. Darcy velocity is calculated by referring the flow rate to the total cross-section; due to channeling effects at the walls of the box this does not give the correct Darcy velocity at the centre of the packed bed but a value which is approximately 4% too high [11].

4. Estimation of dispersion coefficients

4.1. Ordinary least squares

Thermal dispersion coefficients will be estimated from temperature response measurements. These temperatures, taken at n positions (x_i, y_i) and m times t_k, are set into a column vector $\mathbf{T}^{\exp}$. The underlying theoretical model depends on the unknown parameters $(\lambda_x, \lambda_y, \ldots)$, set into vector $\boldsymbol{\beta}$, and yields the corresponding theoretical vector $\mathbf{T}(\boldsymbol{\beta})$. In the ideal case where the model is true, experimental data differ from the theoretical curves only by additive measurement noise $\boldsymbol{\epsilon}$. Parameters can then be estimated by minimizing the sum of squares

$$S(\boldsymbol{\beta}) = (\mathbf{T}^{\exp} - \mathbf{T}(\boldsymbol{\beta}))^{\mathrm{T}}(\mathbf{T}^{\exp} - \mathbf{T}(\boldsymbol{\beta})) \tag{8}$$

using the Gauss iteration algorithm

$$\mathbf{b}_{k+1} = \mathbf{b}_k + (\mathbf{X}^{\mathrm{T}}(\mathbf{b}_k)\mathbf{X}(\mathbf{b}_k))^{-1}\mathbf{X}^{\mathrm{T}}(\mathbf{b}_k)(\mathbf{T}^{\exp} - \mathbf{T}(\mathbf{b}_k)) \tag{9}$$

Here $\mathbf{X} = \frac{\partial \mathbf{T}}{\partial \boldsymbol{\beta}}$ denotes the sensitivity matrix the columns of which are partial derivatives of the theoretical temperature. In this way, a parameter estimate $\widehat{\boldsymbol{\beta}}$ is obtained which contains a stochastic error due to measurement noise and additionally may be biased; in the case of normal measurement noise we have

$$\mathbf{cov}(\widehat{\boldsymbol{\beta}}) \approx (\mathbf{X}^{\mathrm{T}}(\widehat{\boldsymbol{\beta}})\mathbf{X}(\widehat{\boldsymbol{\beta}}))^{-1}\mathbf{cov}(\boldsymbol{\epsilon}) \tag{10}$$

We are using here the notation and results of Beck [12].

As pointed out in the previous section, neither water velocity nor thermocouple positions are precisely known; to avoid erroneous estimation of the thermal dispersion coefficients, these parameters should be estimated simultaneously. In (classical) least squares estimation from axial measurements ($y_i = 0$), only the following three estimation modes are possible, otherwise the parameters become correlated:

$$\boldsymbol{\beta}_1 = [\,\lambda_x \quad \lambda_y\,]^{\mathrm{T}} \tag{11}$$

$$\boldsymbol{\beta}_2 = [\,\lambda_x \quad \lambda_y \quad u\,]^{\mathrm{T}} \tag{12}$$

$$\boldsymbol{\beta}_3 = [\,\lambda_x \quad \lambda_y \quad \mathbf{x}^{\mathrm{T}}\,]^{\mathrm{T}} \tag{13}$$

Here $\mathbf{x}$ is a column vector containing all x-positions.

4.2. Gauss–Markov estimation

If velocity and positions are to be estimated at the same time

$$\boldsymbol{\alpha}_4 = [\,\lambda_x \quad \lambda_y \quad u \quad \mathbf{x}^{\mathrm{T}}\,]^{\mathrm{T}} \tag{14}$$

we need to use prior information on the thermocouple locations. Their nominal positions x_i^{nom} (before the glass beads are filled in the box) can be taken as a complementary measurement signal, and a new signal vector $\mathbf{Y}$ as well as its theoretical counterpart $\boldsymbol{\eta}$ can be defined

$$\mathbf{Y} = \begin{bmatrix} \mathbf{T}^{\mathrm{exp}} \\ \mathbf{x}^{\mathrm{nom}} \end{bmatrix}, \quad \boldsymbol{\eta}(\boldsymbol{\alpha}_4) = \begin{bmatrix} \mathbf{T}(\boldsymbol{\alpha}_4) \\ \mathbf{x} \end{bmatrix} \tag{15}$$

The sum of squares is extended to comprise temperatures and positions

$$\widetilde{S}(\boldsymbol{\alpha}_4) = (\mathbf{Y} - \boldsymbol{\eta}(\boldsymbol{\alpha}_4))^{\mathrm{T}} \boldsymbol{\Omega}^{-1} (\mathbf{Y} - \boldsymbol{\eta}(\boldsymbol{\alpha}_4)) \tag{16}$$

and contains the weighting matrix

$$\boldsymbol{\Omega} = \begin{bmatrix} \sigma_{\mathrm{T}}^2 \mathbf{I}_{n\cdot m} & \mathbf{0} \\ \mathbf{0} & \sigma_{\mathrm{pos}}^2 \mathbf{I}_n \end{bmatrix} \tag{17}$$

where σ_{T} is the standard deviation of temperature measurement noise and σ_{pos} the standard deviation of (normal) thermocouple wire displacement. $\widetilde{S}$ can also be alternatively written as the classical least square sum S that has been associated with a penalization term based on locations, with weighting factors that are the square of standard deviations of temperatures and locations:

$$\widetilde{S}(\boldsymbol{\alpha}_4) = \frac{1}{\sigma_{\mathrm{T}}^2} S(\boldsymbol{\alpha}_4) + \frac{1}{\sigma_{\mathrm{pos}}^2} (\mathbf{x}^{\mathrm{nom}} - \mathbf{x})^{\mathrm{T}} (\mathbf{x}^{\mathrm{nom}} - \mathbf{x}) \tag{18}$$

Minimization of this new sum of squares corresponds to Gauss–Markov estimation [12] and is achieved by the algorithm

$$\mathbf{a}_{k+1} = \mathbf{a}_k + (\widetilde{\mathbf{X}}^{\mathrm{T}}(\mathbf{a}_k) \boldsymbol{\Omega}^{-1} \widetilde{\mathbf{X}}(\mathbf{a}_k))^{-1} \widetilde{\mathbf{X}}^{\mathrm{T}}(\mathbf{a}_k) \boldsymbol{\Omega}^{-1} (\mathbf{Y} - \boldsymbol{\eta}(\mathbf{a}_k)) \tag{19}$$

which generalizes Eq. (9) and employs the sensitivity matrix $\widetilde{\mathbf{X}} = \frac{\partial \boldsymbol{\eta}}{\partial \boldsymbol{\alpha}_4}$. The estimation error can be given as

$$\mathbf{cov}(\widehat{\boldsymbol{\alpha}}_4) \approx (\widetilde{\mathbf{X}}^{\mathrm{T}}(\widehat{\boldsymbol{\alpha}}_4) \boldsymbol{\Omega}^{-1} \widetilde{\mathbf{X}}(\widehat{\boldsymbol{\alpha}}_4))^{-1} \tag{20}$$

The value of σ_{pos} is not exactly known, but estimation results are independant of its choice for a wide range [13].

Thermocouple positions can be estimated in two dimensions if they are placed slightly off-axis ($y_i^{\mathrm{nom}} = 2.5$ mm) to have a non-zero sensitivity to the y-position and still a big enough temperature signal. The extension of the parameter vector and its estimation is straightforward:

$$\boldsymbol{\alpha}_5 = [\,\lambda_x \quad \lambda_y \quad u \quad \mathbf{x}^{\mathrm{T}} \quad \mathbf{y}^{\mathrm{T}}\,]^{\mathrm{T}} \tag{21}$$

5. Monte Carlo simulation of experiments

In order to assess estimation errors, experiments with thermocouples 2–7 were simulated by the Monte Carlo method [12]. Here, we only discuss our results for the high reference velocity [10]. The error on measurement locations was simulated by adding random normal noise of standard deviation σ_{pos} to the nominal positions; this means that the nominal (imposed) positions differ from the exact positions by a "noise" of standard deviation σ_{pos}. The exact water velocity was taken 4% below its nominal value. Then, theoretical temperatures were calculated at times $t_k = 0.15, 0.3, 0.45, \ldots, 45$ s, and random normal noise of standard deviation $\sigma_{\mathrm{T}} = 0.02$ K was added. From these simulated experimental data, parameters were estimated by the different modes, using nominal values for "measured" velocity and positions. To obtain significant results, 400 such measurements were simulated (with new thermocouple locations in each simulation); finally, for every estimated parameter its mean value and the statistical standard deviation were calculated.

Table 3 shows a comparison of the ordinary least squares modes $\boldsymbol{\beta}_i$ with Gauss–Markov estimation $\boldsymbol{\alpha}_4$; thermocouples are located on the x-axis and no noise is added in y-direction. (The estimated positions are given relative to the exact positions.) One can clearly see, that

Table 3
Estimation results for Monte Carlo simulations for axial measurements ($y_i = 0$), with unknown velocity (whose exact value is $u = 6.288$ mm s^{-1}) and with stochastic errors added to the nominal x-positions ($\sigma_{\mathrm{pos}} = 2$ mm)

	$\boldsymbol{\beta}_1$	$\boldsymbol{\beta}_2$	$\boldsymbol{\beta}_3$	$\boldsymbol{\alpha}_4$
$\hat{\lambda}_x$ (W m^{-1} K^{-1})	68.50 ± 2.16	60.85 ± 1.54	65.07 ± 0.74	60.02 ± 1.14
$\hat{\lambda}_y$ (W m^{-1} K^{-1})	2.903 ± 0.067	2.999 ± 0.081	2.765 ± 0.005	2.999 ± 0.050
$\hat{u}$ (mm s^{-1})	–	6.293 ± 0.056	–	6.290 ± 0.052
$\hat{x}_2 - x_2$ (mm)	–	–	1.67 ± 0.12	0.01 ± 0.35
$\hat{x}_3 - x_3$ (mm)	–	–	2.48 ± 0.14	0.00 ± 0.51
$\hat{x}_4 - x_4$ (mm)	–	–	3.33 ± 0.17	0.02 ± 0.66
$\hat{x}_5 - x_5$ (mm)	–	–	4.16 ± 0.19	0.02 ± 0.83
$\hat{x}_6 - x_6$ (mm)	–	–	4.94 ± 0.21	-0.02 ± 1.04
$\hat{x}_7 - x_7$ (mm)	–	–	5.82 ± 0.26	0.03 ± 1.16

The exact dispersion coefficient values are $\lambda_x = 60$ W m^{-1} K^{-1} and $\lambda_y = 3$ W m^{-1} K^{-1}.

mode $\boldsymbol{\alpha}_4$ outperforms the classical modes by yielding small estimation errors and no significant bias for all estimated parameters.

However, in real experiments, thermocouple positions are inaccurate in *two* dimensions. Monte Carlo simulations reveal that this can lead to large estimation errors in mode $\boldsymbol{\alpha}_4$ where the error on y-positions is not compensated. Fig. 6 shows the results in direct comparison with those of mode $\boldsymbol{\alpha}_5$ in off-axis geometry (cf. Fig. 4b). Concerning the estimation of the longitudinal dispersion coefficient λ_x, Darcy velocity u and x-positions, mode $\boldsymbol{\alpha}_5$ clearly gives the better results. In contrast, estimation of the lateral dispersion coefficient λ_y, for which mode $\boldsymbol{\alpha}_4$ systematically yields too big values, is of even poorer quality in mode $\boldsymbol{\alpha}_5$: the estimated values are now too small and widely dispersed. Furthermore, y-values are overestimated in mode $\boldsymbol{\alpha}_5$, which can be explained by a strong correlation of λ_y and y_i [10].

6. Experimental results for three different geometries

6.1. Axial measurements with line heat source

Typical experimental temperatures for (axial) thermocouples are plotted in Fig. 7a. All data points were

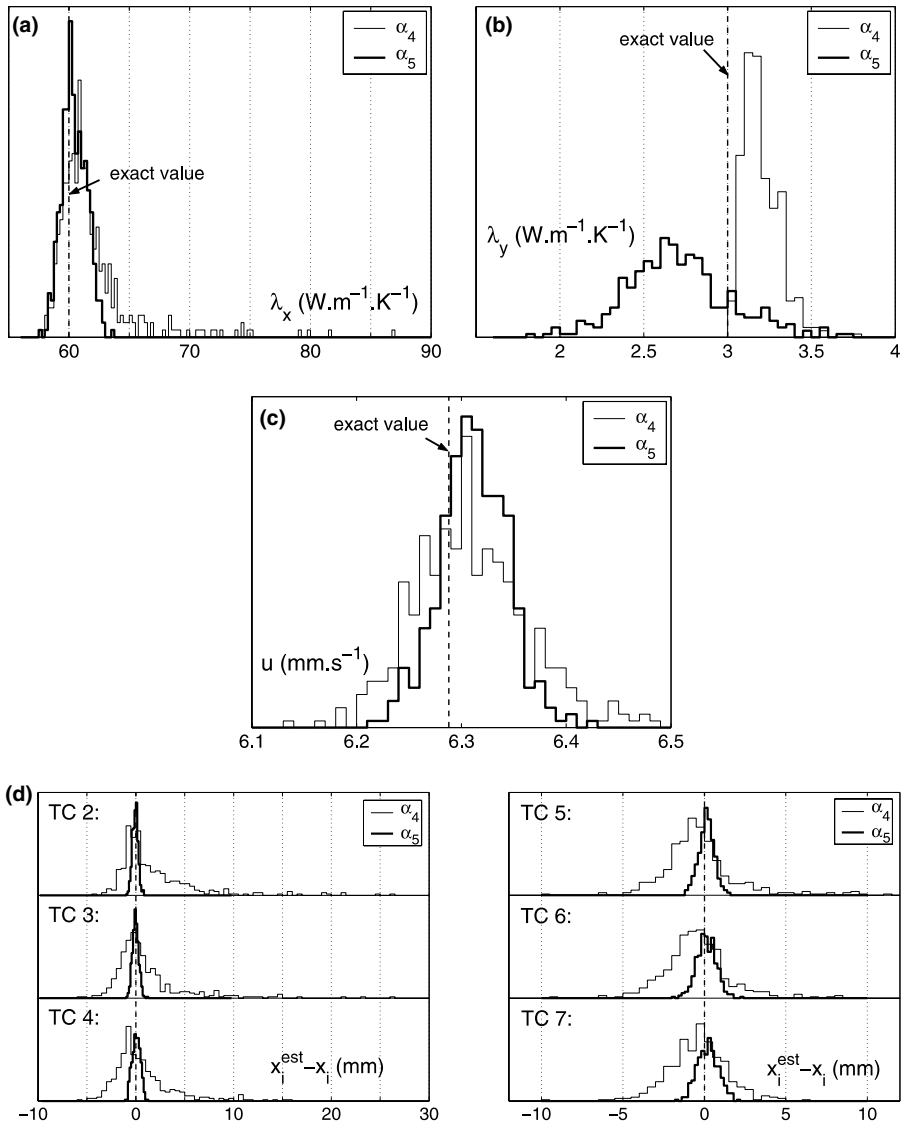

Fig. 6. Histograms for Monte Carlo simulations comparing axial measurements ($y_i^{\text{nom}} = 0$) and estimation mode $\boldsymbol{\alpha}_4$ with off-axis measurements ($y_i^{\text{nom}} = 2.5$ mm) and estimation mode $\boldsymbol{\alpha}_5$ (in both cases, $\sigma_{\text{pos}} = 1$ mm in two dimensions).

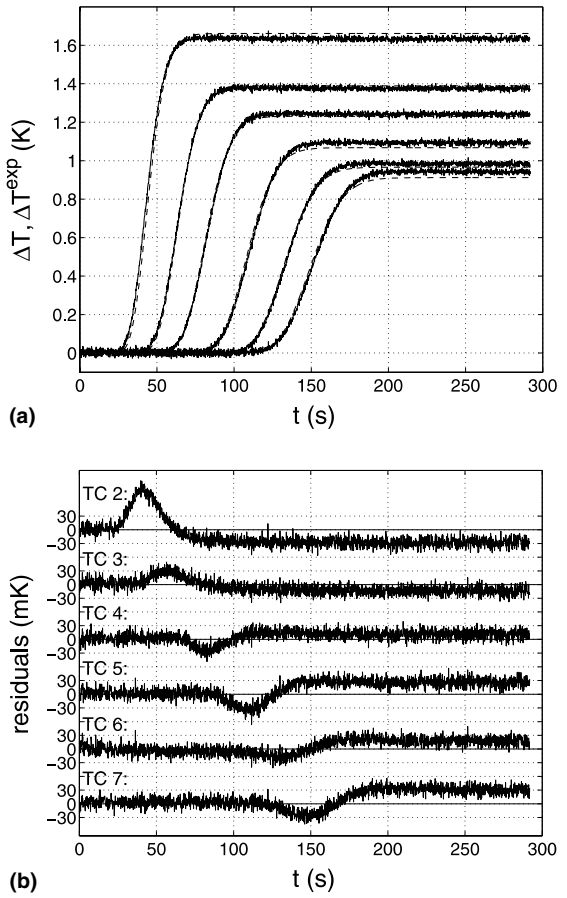

Fig. 7. Transient temperature response at low reference water velocity for axially-positioned thermocouples 2–7 (a) and magnified residuals for mode $\boldsymbol{\alpha}_4$ (b).

used to estimate the parameter vector $\boldsymbol{\alpha}_4$: the recalculated temperatures are given as slashed lines. The residuals (Fig. 7b) are correlated due to uncompensated error on y_i.

Estimation results for thermal dispersion coefficients, water velocity and x-positions are shown in Figs. 8 and 9. The velocity dependence of λ_x and λ_y will be discussed later. Concerning water velocity, we find the estimated value (based on data from the center of the packed bed) to be a few percent smaller than the measured value (average over cross section), which can be explained by channeling effects. For small Péclet numbers, this difference increases, probably due to natural convection which slows down water flow in the neighborhood of the heating wire. The estimated x-positions depend strongly on water velocity in this experimental situation where the thermocouple locations are unknown but velocity independent; the reason for this effect is again the uncompensated error on y-positions [10].

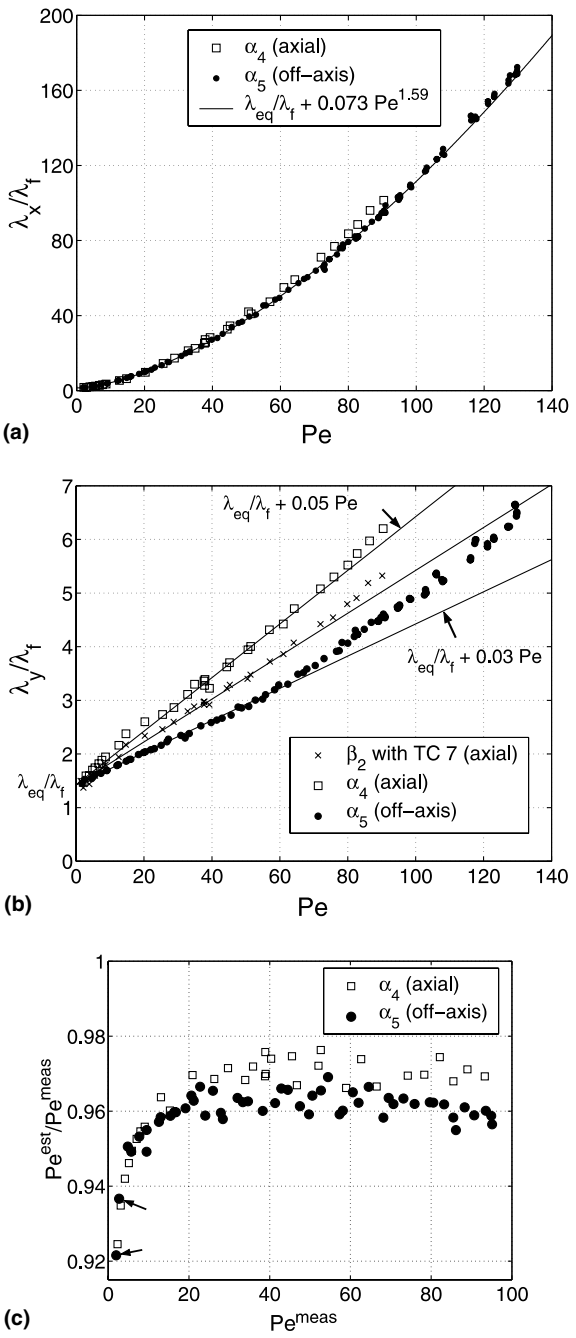

Fig. 8. Estimated thermal dispersion coefficients and Darcy velocity for different measurement geometries and estimation modes.

6.2. Off-axis measurements with line heat source

Fig. 10 represents experimental temperature data from thermocouples that are set off-axis ($y_i^{\text{nom}} = 2.5$ mm) for the high reference velocity. (In this geometry,

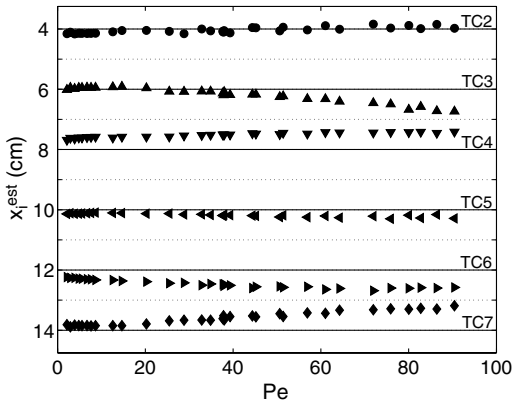

Fig. 9. Estimated thermocouple positions for axial measurements and estimation mode α_4.

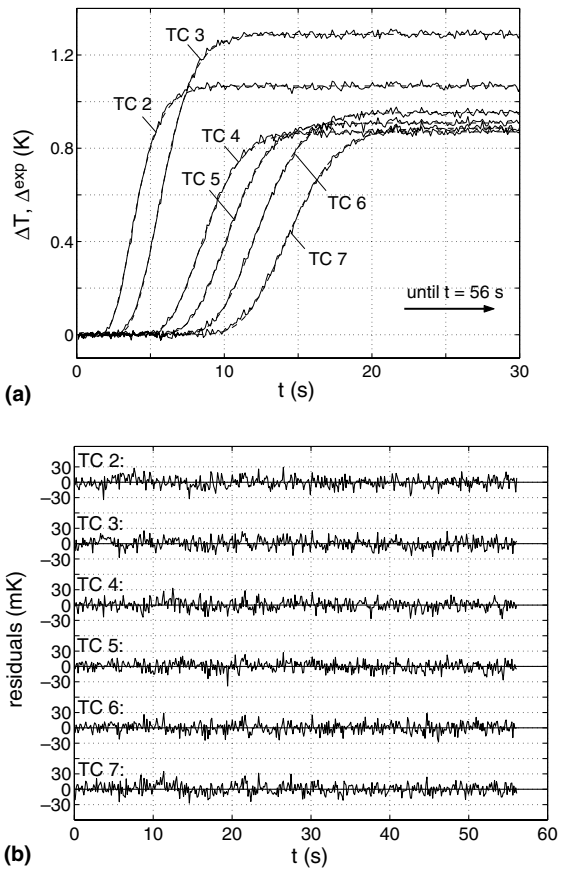

Fig. 10. Transient temperature response at high reference water velocity for thermocouples 2–7 set off-axis (a) and residuals for estimation mode α_5 (b).

stationary temperature levels may be interchanged.) Parameters are estimated in mode α_5 yielding excellent residuals with no observable correlation.

Thermal dispersion estimation results are shown in Fig. 8; for the longitudinal coefficient λ_x both estimation modes α_4 and α_5 yield similar values whereas the results for λ_y differ very much. This is in perfect accordance with our Monte Carlo simulations which showed that λ_y is overestimated in axial mode α_4 and underestimated in off-axis mode α_5. As to the longitudinal dispersion coefficient λ_x, they suggest the results of mode α_5 to be highly reliable, so that we correlated them using a power law [10]. Here $\lambda_{eq} \approx 0.86\ \mathrm{W\,m^{-1}\,K^{-1}}$ is the equivalent thermal conductivity of the packed bed with no flow.

Concerning the lateral dispersion coefficient λ_y, we only give upper and lower limits, and also display estimation results of mode β_2 using only data from thermocouple 7 for which errors on the position are less important. Regarding to water velocity, mode α_5 in the whole confirms the results of axial estimation mode α_4 (See Fig. 8c where the ratio of the estimated—through thermocouple measurements—over measured—by flowmeter—velocities is plotted as a function of the measured Péclet number constructed with this last velocity).

Estimated thermocouple positions are plotted in Fig. 11 for all off-axis experiments along with the nominal positions; a representative glass bead (circle) illustrates the dimensions. Apart from the two experiments at $Pe < 3$ with significant natural convection (empty circles, see arrows pointing at filled circles in Fig. 8c) the results display only a weak velocity dependence, greatly reduced in comparison with axial mode α_4. These results also show that no visible bias appears since the estimated locations seem to be evenly scattered in all directions around their nominal locations.

6.3. Measurements with plane heat source

In plane heating, only the longitudinal dispersion coefficient can be estimated (one-dimensional geometry). Unfortunately, plane heating power W is not precisely known because the distance between the heating elements could not be perfectly controlled. There are two ordinary least squares estimation modes [10]:

$$\boldsymbol{\beta}_{\mathrm{I}} = [\,\lambda_x \quad u \quad \mathbf{x}^{\mathrm{T}}\,]^{\mathrm{T}} \tag{22}$$

$$\boldsymbol{\beta}_{\mathrm{II}} = [\,\lambda_x \quad u \quad W\,]^{\mathrm{T}} \tag{23}$$

Not all four parameters (λ_x, u, x_i and W) can be estimated simultaneously because they are perfectly correlated. Thus, estimation is always based on imprecise information and cannot be expected to be of high quality. Fig. 12 shows estimation results for the two modes which on the whole confirm our correlation obtained from off-axis estimation.

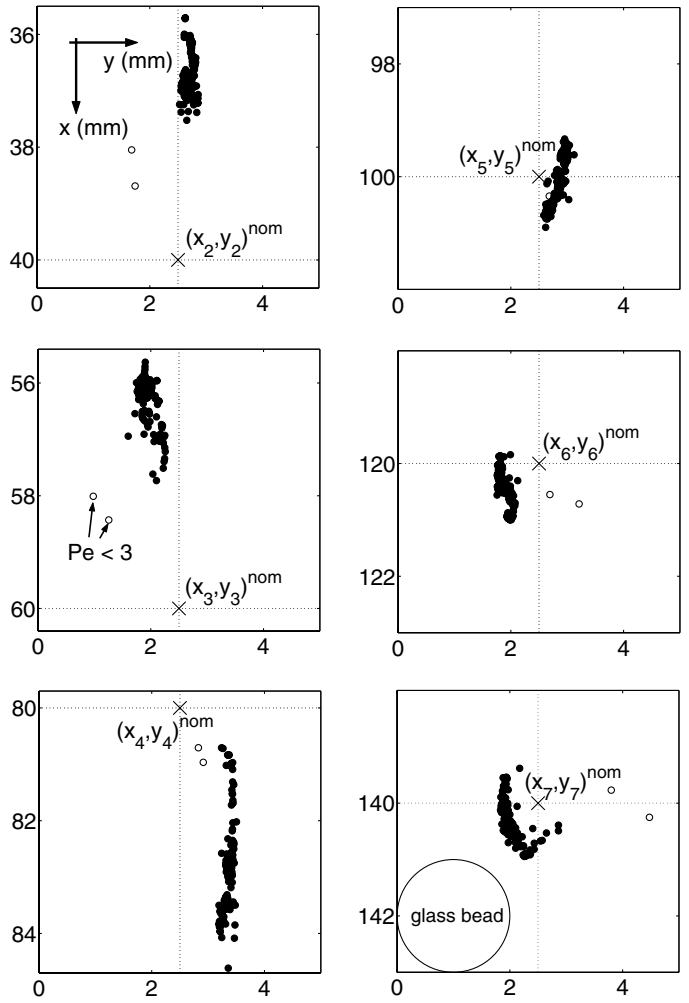

Fig. 11. Estimated thermocouple positions for off-axis measurements and estimation mode α_5.

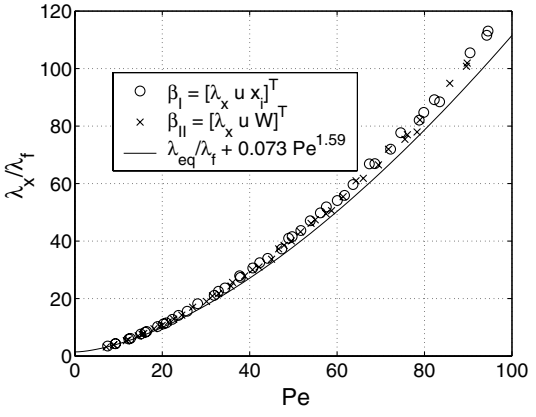

Fig. 12. Estimation results for experiments with plane heat source.

7. Discussion

In Fig. 13 our results for the longitudinal thermal dispersion coefficient λ_x are compared to experimental data from Green [8] as well as from Levec and Carbonell [9], to numerical results of Da Silveira [7] and to the model of Tsotsas [1]; to this purpose the power law correlation is plotted for an extended range of Péclet numbers. We find our results validated by Green who used exactly the same solid-fluid system. The data of Levec and Carbonell are different in absolute values—probably due to their different values of ε and $(\rho c_p)_s$—but display the same logarithmic slope as our results. This holds also for Da Silveira's numerical findings, obtained for a two-dimensional system with fluid and solid phase having identical thermal properties. The model of Tsotsas has a slightly different logarithmic behaviour but predicts very well our results for $Pe > 70$.

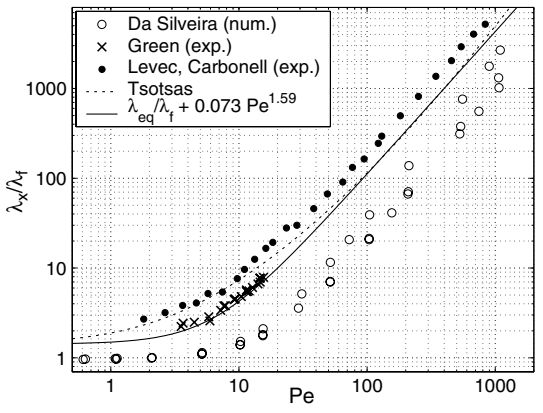

Fig. 13. Longitudinal thermal dispersion coefficient λ_x: this work and literature.

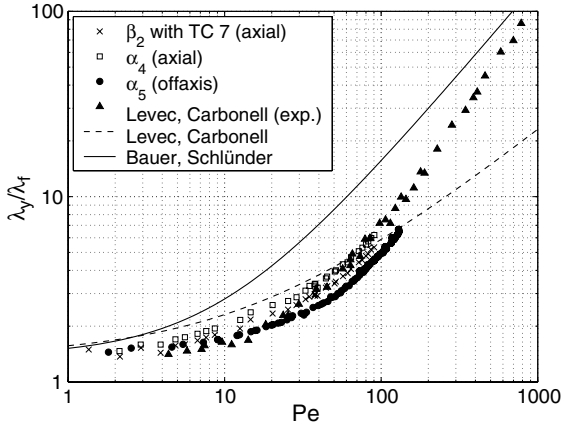

Fig. 14. Lateral thermal dispersion coefficient λ_y: this work and literature.

Our results for the lateral thermal dispersion coefficient λ_y, obtained from three different estimation modes, are plotted in Fig. 14 together with the model of Bauer and Schlünder [2] and the results of Levec and Carbonell [9]. Despite the problem of estimation errors, our values are confirmed by the experimental data of Levec and Carbonell who used a completely different experimental set-up. Their theoretical model is based on mass dispersion and can describe neither their experiments nor our results. The model of Bauer and Schlünder gives much higher values than ours—probably due to their assumption of perfect mixing in the pores.

8. Conclusion

A minimally intrusive experimental technique for thermal dispersion characterization in packed beds has been presented. The small temperature signal ($\Delta T \approx 1$ K) is produced by a heating wire and measured by thermocouples, both in the central region of the packed bed to avoid wall effects. By a special choice of measurement locations (off-axis) and Gauss–Markov type parameter estimation (mode α_5), experimental difficulties linked to uncertainties on thermocouple exact positions and on Darcy velocity have been successfully overcome. Monte Carlo simulations show that our results for the longitudinal thermal dispersion coefficient λ_x are of high quality; the lateral coefficient λ_y can be estimated simultaneously but with lower accuracy.

Our results for $\lambda_x(Pe)$ correspond to a power law with an exponent of approximately 1.6 and are in good agreement with literature data. Concerning λ_y, we obtain significantly lower values than those predicted by the widely-used model of Bauer and Schlünder [2]; however, the linear dependence with the Péclet number seems to be confirmed.

Excellent temperature residuals up to high Péclet numbers (see Fig. 10) suggest that the one-temperature model may also be used in the case of local thermal non-equilibrium. Great attention was paid to the experimental estimation of a high number of parameters (dispersion coefficients, a velocity and six thermocouple positions): their estimated values do not only serve in a mathematical curve fitting exercise but also have to yield physically reasonable and intrinsic values. Three different experimental geometries could confirm the results for λ_x.

The fact that the measured temperature is probably closer to the fluid temperature $\langle T_f \rangle^f$ than to that of the one-temperature model $\langle T \rangle$ poses no problem: the analysis of Carbonell and Whitaker [3] shows that the longitudinal dispersion coefficient is equal for both phases.

This work is currently continued to apply the presented technique to gas flow through porous media; thus, the one-temperature model can be tested for two phases with very different thermal properties. First results for a packed bed of glass beads are very promising, they will be published in due time. Future work will implement more precise experimental estimation of the lateral dispersion coefficient to validate the above results.

References

[1] E. Tsotsas, Über die Wärme- und Stoffübertragung in durchströmten Festbetten, Fortschrittberichte, Reihe 3, Nr. 223, VDI, Düsseldorf, 1990.

[2] R. Bauer, E.-U. Schlünder, Effective radial thermal conductivity of packings in gas flow. Part I: convective transport coefficient, Int. Chem. Eng. 18 (1978) 181–188.

[3] R.G. Carbonell, S. Whitaker, Heat and mass transfer in porous media, in: J. Bear, M.Y. Corapcioglu (Eds.), Fundamentals of Transport Phenomena in Porous Media, Nijhoff, 1984, pp. 122–198.
[4] J.L. Auriault, P.M. Adler, Taylor dispersion in porous media: analysis by multiple scale expansions, Adv. Water Resour. 18 (1995) 217–226.
[5] M. Quintard, M. Kaviany, S. Whitaker, Two-medium treatment of heat transfer in porous media: numerical results for effective properties, Adv. Water Resour. 20 (1997) 77–94.
[6] C. Moyne, S. Didierjean, H.P. Amaral Souto, O.T. Da Silveira, Thermal dispersion in porous media: one-equation model, Int. J. Heat Mass Transfer 43 (2000) 3853–3867.
[7] O.T. Da Silveira, Thermal dispersion in periodic porous media: a numerical study, Ph.D. thesis, UERJ-IPRJ Nova Friburgo, Brazil, 2001 (in Portuguese).
[8] D.W. Green, R.H. Perry, R.E. Babcock, Longitudinal dispersion of thermal energy through porous media with a flowing fluid, AIChE J. 10 (1964) 645–651.
[9] J. Levec, R.G. Carbonell, Longitudinal and lateral thermal dispersion in packed beds, AIChE J. 31 (1985) 581–601.
[10] T. Metzger, Thermal dispersion in porous media: experimental characterisation by inverse technique, Ph.D. thesis, INPL Nancy, France, 2002 (in French).
[11] M. Winterberg, Modellierung des Wärme- und Stofftransports in durchströmten Festbetten mit homogenen Einphasenmodellen, Fortschritt-Berichte, Reihe 3, Nr. 654, VDI, Düsseldorf, 2000.
[12] J.V. Beck, K.J. Arnolds, Parameter Estimation in Engineering and Science, John Wiley & Sons, New York, 1977.
[13] T. Metzger, S. Didierjean, D. Maillet, Integrating the error in the independant variable for optimal parameter estimation—part II, Inverse Problems Engng. 11 (2003) 175–186.